Optical and Quantum Electronics (2023) 55:1190
https://doi.org/10.1007/s11082-023-05496-z

Tuning the TiO_2/ZnO heterostructures emissions through nickel doping for intriguing optoelectronic and photonic applications

Amine El Haimeur[1,3] · Maryama Hammi[2] · Paloma Fernández Sánchez[4] · Hicham Bakkali[1] · Eduardo Ollero Blanco[1] · Abdelmalek Ouannou[5] · Abdellah Laazizi[6] · Manuel Domínguez de la Vega[1] · Khalid Nouneh[3] · Adil Echchelh[7]

Received: 28 June 2023 / Accepted: 26 September 2023 / Published online: 17 October 2023

Abstract
It opens the door to many optoelectronic and photonic applications. Here, synthesized TiO_2 was deposited on Ni(0,8,10,12%) doped ZnO using two different methods; TiO_2 was coated on Ni(0,8,10,12%) prepared by dip coating. 12%) doped on top of ZnO, and Ni-doped ZnO films were grown by spray pyrolysis. Analysis of surface structure was conducted using Atomic Force Microscopy, scanning electron microscopy and microscopic Raman spectroscopy. Nickel doping was investigated by EDS analysis to ensure that the incorporation of dopants does not form a second phase. In addition, spectroscopic measurements including UV–Vis absorption and photoluminescence were performed. Preliminary results show that Ni doping reduces the absorption of TiO_2/ZnO in the visible region. The carbon content is shown in the form of photoluminescence with a maximum of green, orange and red. Therefore, TiO_2/Ni-doped ZnO heterostructures can also be used to exploit these findings in nanophotonics applications.

Keywords ZnO/TiO_2 · Heterostructures · LED · Nanophotonics · Optoelectronic devices

1 Introduction

Metal oxide materials have attracted tremendous attention due to their fascinating properties and easy integration. These materials promote device fabrications used in many technological applications (Sisman et al. 2017; Nikoobakht et al. 2013; Moyen et al. 2020). N-type ZnO Semiconductor oxides such as CuO/ZnO were used in the photodetector Diodes, as junctions using thin layers of zinc oxide Homo-Junction to produce light emitting diodes and thus to improve efficiency of the LED device (Cuesta et al. 2019) [3.5–7]. Additionally, it has been discovered that Zinc oxide is effective when doped with Nickel in a variety of nanoforms, such as nanorod hole transporting layers (HTLs) in solar cell applications (Moyen et al. 2020; Hanada 2009; Look 2004; Chen and Yang 2016) and nanoparticles in LED applications (Elilarassi and Chandrasekaran 2010). ZnO is then still a possibility for boosting light output power (Son et al. 2018). ZnO has focused a lot of

Extended author information available on the last page of the article

efforts owing to its mesmerizing properties, versatility, ease of processing, manufacturing and wideband gap. In addition, many works have been devoted to using different elements for doping these materials in order to tune their properties pursuing new milestone results in the field of LED applications. Huge endeavors in this sense were carried out to develop methods for growing integrated zinc oxide thin films in many electronic and optical devices, such as waveguide devices and based quantum dots have been stacked to improve the efficiency of solar cells (Rahman 2019; Manekkathodi et al. 2013; Yin et al. 2013). It was previously stated that the preparation and deposition of ZnO synthesized into real devices is difficult in some cases and necessitates additional modifications such as foreign doping, the creation of a ZnO composite, or defects engineering in order to achieve optimal performance (Harun et al. 2017). Accordingly, it was shown by Kityk et al. (2002) that fluorine-doped wurtzite-type ZnO layers deposited on bare glass had the potential to significantly enhance the linear electro-optic effect. The obtained values of second and third order nonlinear susceptibilities were found to be sufficient for the potential applications of the investigated materials in the optical switching devices based on refractive index changes in another significant study by Waszkowska et al. (2021).

Potential optoelectronic and photonic applications are revealed by the outstanding NLO results reported elsewhere (Kulyk 2007).This fact was assessed through structural and optical properties of ZnO thin films deposited using pulsed laser deposition technique on quartz substrates, and the susceptibilities were found to be high enough for potential applications in optical switching devices, and the ability to tailor the NLO response to the needs of particular applications is very encouraging in the direction of using these materials for photonic applications (Zawadzka et al. 2016).

Asib et al. findings revealed a good yield in terms of light emission, particularly because of the blue shift emissions compared to the ZnO layer, which changes to red or blue in the UV range. Other target emissions colors remain a key technological. Among the oxides used, we can find ZnO materials, implemented in LED devices and as multiple quantum wells (MQWs), etc. (Asib et al. 2016; Binbin et al. 2020; Huang et al. 2016). For instance, by stacking TiO_2 and ZnO, Chen et al. were able to create a high-performance white QD-LED while exploring the white color. For this reason, many methods have been used for depositing ZnO materials; such as pulsed laser deposition, atomic layer epitaxy, sol–gel spin coating, etc. Among these aforementioned techniques, Spray techniques and dip-coating remain simple and inexpensive processing methods, using small amounts of precursors and requiring a few minutes for sample preparation. In this work, we will investigate the properties of ZnO-TiO_2 heterostructures such as LED applications and optoelectronics by shedding light on the preparation processes and the role of Ni doping in tuning the microstructure, absorbance and emission in visible range (Chen et al. 2014; Hong et al. 2015; Blanco et al. 2015).

2 Materials and methods

2.1 Experimental procedure

Ni-doped ZnO thin films have been prepared using the Spray pyrolysis technique; A spray gun, a ceramic base heater with a Kanthol coil heating element, and a temperature controller make up the spray pyrolysis experimental setup used for film deposition. As a hot plate and substrate holder, a circular stainless steel plate retained on the heater assembly was

used. A REX—F900 PID digital temperature controller, with an inaccuracy of 5 °C, is used to regulate the temperature. The spraying was done with a double-nozzle spray cannon made of glass. A coaxial combination of quartz tube and capillary makes up the spray cannon. The quartz tube is utilized to transmit the carrier gas, while the capillary serves as the input for the solution.

In order to completely cover the substrate surface, the distance between the spray gun and the substrate was adjusted. In order to make zinc oxide, zinc acetate ($Zn(COOH_3)_2$) was used as a precursor. In order to dissolve the minor precipitates and make the solution transparent, this precursor was dissolved in distilled water/Methanol and acetic acid. The formation of hydroxides can also be avoided with the help of acetic acid. It's important to note that each film was deposited five times, and the results showed that the films can be reproduced.

TiO_2 films have been deposited using the sol–gel dip coating process, titanium dioxide (TiO_2) thin films were prepared. Initially, 1 ml of tetraethyl orthosilicate (TEOS) solution was mixed in 50 ml of ethanol, and stirring at 30 °C for 30 min, then 0.125 g of TiO_2 powders which were calcined at different temperature from 500 to 800 °C were dispersed in this solution, and stirring for 1 h, following by sonication for 5–10 min to disperse the TiO_2 powders to be homogeneous colloid solution which was used as precursor for dip coating. The cleaned glass substrates were dipped into the solution for one minute at a pace of one millimeter per second. The coated films were allowed to dry at 100 °C for 5 min after each coating cycle. Afterwards TiO_2 were stacked on the as-prepared Ni(0,8, 10, and 12%-doped ZnO films using the sol–gel process. It's worth mentioning that the growing process of the nanostructure of TiO_2 thin layers have already been described Haimeur et al. 2020, 2021; Frank et al. 2012).

2.2 Characterization

Micro-photoluminescence (μ-PL) and Raman experiments were performed at room temperature in a Horiba Jovin Yvon Lab RAM HR800 confocal microscope with a He-Cd ($\lambda ex = 325$ nm) or He–Ne ($\lambda ex = 632.8$ nm) laser as excitation source, respectively.

Optical absorption spectra of all films have been performed using a Shimadzu UV-1603 spectrophotometer. The surface topography of the films was characterized by atomic force microscopy (AFM) (with tapping-mode Atomic Force Microscopy (T-AFM, Bruker Multimode IIIa Nanoscope). In addition, the microstrucres and nanostructures distribution, of the samples, have been performed using the SM-IT500HRLA Scanning Electron Microscope. In addition, EDS atomic mapping and EDS elemental composition have been carried out.

3 Results and discussions

3.1 Raman spectrum

Raman spectroscopy is considered a suitable experimental technique for revealing information about the structural arrangement of atoms. That vibrational spectroscopy technique measures Raman and vibrational states and provides information about the crystallinity of the studied materials. Currently, the use of this vibrational spectroscopy has developed strongly for the characterization of semiconductor materials. It has been used to measure

the deformation in a device or in a semiconductor material since it is sensitive to the variation of the lattice parameters.

Raman spectra of the films were recorded in the range of 100–1000 cm^{-1} to investigate the structural features of the Ni-doped films. The obtained spectra show the dominant hexagonal ZnO phonon modes at 100, 385, 440 and 585 cm^{-1} (see Fig. 1). On the other hand, the peak around 570 cm^{-1} is associated with Ni doping (Owoeye 2019); note that the amounts of metal transition elements are represented in weight percent.

The doping of Ni obviously influences the corresponding Raman profiles, which suggests that the structure of the matrix was altered by the nature of doped metal particles. Indeed, the peaks tend to increase and broaden after increasing the rate of Ni doping inside the hexagonal lattices and depending on the impurities rate. The peak at 570 belongs to the A(01) mode, indicating the presence of Ni impurities in the hexagonal lattice of ZnO. It should be noted that the representative main peak Raman spectrum of anatase TiO_2 thin film is shown in Fig. 1. The spectra clearly shows Anatase bands at frequencies of 143.43(Eg)cm^{-1} 399 cm^{-1}(B1g), 516 cm^{-1}(A1g), and 639cm^{-1}(Eg) (Rana et al. 2017) (See Fig. 1.) Ni doping makes it simple to see changes in the entire heterostructure by focusing on the main peaks of both spectra. Indeed, the broadening and intensity peaks of Ni-doped ZnO differ from those of undoped ZnO, and this difference was discovered to be caused by the symmetry alterations brought on by the inclusion of Ni impurities inside the ZnO host lattice (Alvi et al. 2011; Johansson et al. 2019; Rajendraprasad Reddy 2013).

The heterostructure ZnO/TiO_2 film does not show any significant changes in the Raman spectra when it is deposited with doped layers. Since the layers were very thin, it is obviously observed that the intensities of Raman spectra of doped heterostructures are lower than those of undoped heterostructure.

3.2 Surface morphological analysis

The microstructural properties have been investigated by means of SEM(Scanning Electron Microscopy), the images have shown uniform shapes of the above Anatase TiO_2 with the (001) orientations; on top of the Wurtzite ZnO material with a preferential orientation of (002),which supports the Raman spectra results in terms of crystal structures of the

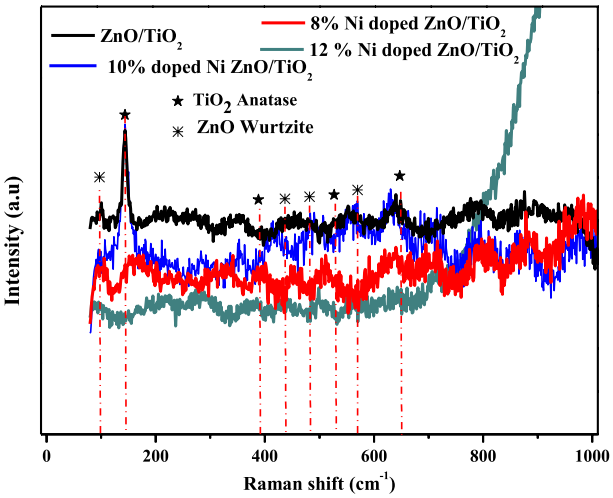

Fig. 1 Raman spectra of TiO_2 on Ni(0,8,10,12%)-doped ZnO heterostructures with main lattices intensities

heterostructures. Meanwhile, the chemical compositions of the heterostructures have been performed using EDS (Energy Dispersive Spectroscopy); thus showing the existence of Ni atoms. It is noteworthy that the Ni elements are mainly present in the Wurtzite lattice, which is in a good agreement with the Raman spectra in terms of crystal structures with any Ni phase formation (see Fig. 4, 5 and 6).

Structural study of the synthesized samples are crucial for disclosing details such as the heterostructure of optoelectronic devices' heterostructure thickness and grain shape. SEM (Scanning Electron Microscopy) was used to perform a depth scan of the sample surface, as shown in Fig. 2. Each sample displayed notably homogenous characteristics and a surface texture. Additionally, all TiO_2 Ni-doped ZnO devices have shaped grains visible in the photos.Moreover, by a cross-section scanning alongside the surface contacts of the Ni-doped TiO_2/ZnO layers, the thickness of the heterostructures was determined. TiO_2 and Ni-doped ZnO thin films' observed thicknesses were therefore estimated to be 325.2 nm and 355 nm, respectively.

3.3 Energy dispersive X-ray spectroscopy and elemental mapping

The elemental analysis of the as prepared thin films was performed by a technique known as Energy Dispersive X-ray (EDS).The emitted X-ray spectrum was recorded in order to determine qualitatively and quantitatively the surface composition of each sample and to ensure the sample compositions. The electron beam energy 20keV was selected for two reasons; the first is because, the maximum X-ray energy collected by the device is 20keV on

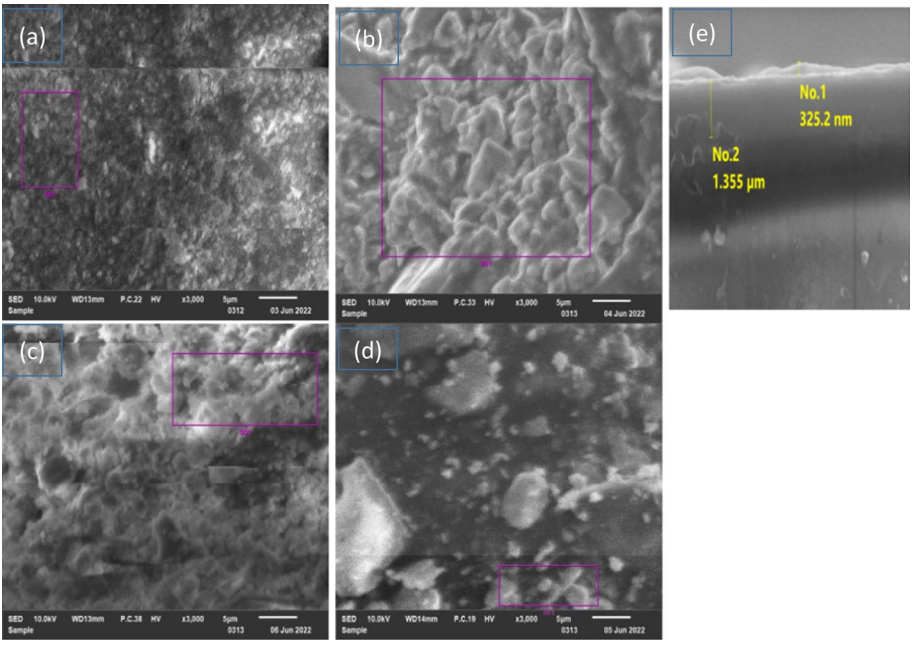

Fig. 2 Scanning Electron Microscopy images of **a** TiO_2/ZnO. **b** TiO_2/8%Ni-doped ZnO. **c**TiO_2/10%Ni-doped ZnO. **d** TiO_2/12%Ni-doped ZnO. **e** cross section images of the TiO_2/Ni-doped ZnO heterostructures devices

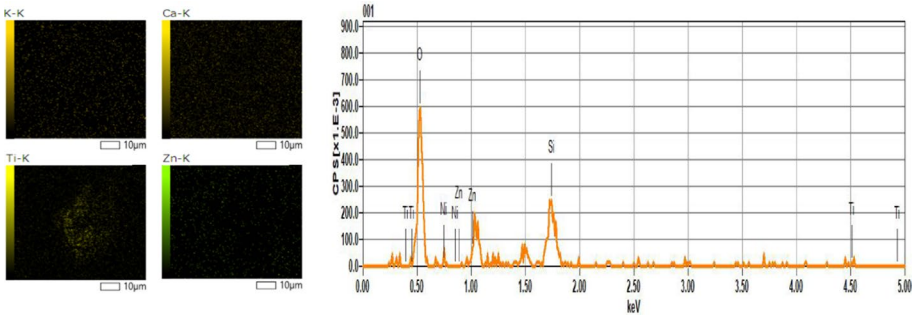

Fig. 3 EDS composition spectra alongside with EDS composition mapping inset, of TiO_2/ Undopped ZnO

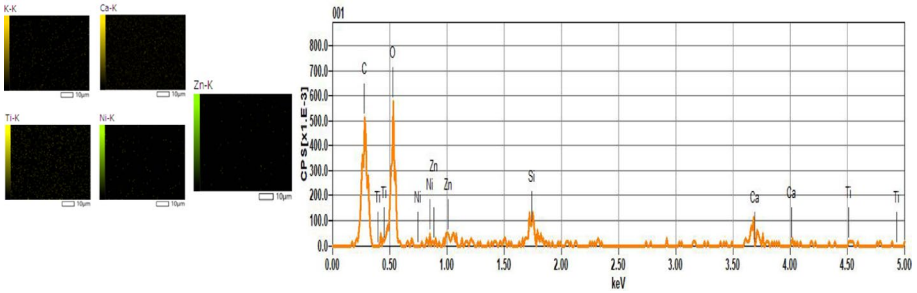

Fig. 4 EDS composition spectra ZnO alongside with EDS composition mapping of TiO_2/8%Ni-doped

the X-ray scale The second reason is to prevent high penetration of the film. The chemical composition allows us the determination of the accurate composition of thin film samples by collecting X-ray from sample at random areas and comparing their results. To assess the presence of all device components and the chemical composition of the samples, the composition of the films was determined by EDS analysis as part of an ongoing study. Further investigation was conducted by mapping the atoms of elements with a high precision scan to shed light on the surface distribution and quantification of each element Devices. Hence, the mean elemental mapping of each Ti, Zn and atomic orbitals K, L, M, etc. was observed, indicating the presence with homogeneous distribution. Moreover, the EDS spectra confirm the presence of the elements of the sample. (See Figs. 3, 4, 5, 6). EDS spectrum presented in Fig. 3 represents the composition of the TiO_2/ Undopped ZnO, the whole marked peaks are assigned to TiO_2/ZnO heterostructure composition. The EDS spectra of TiO_2/ZnO thin films doped with nickel are shown subsequently the every doping rate.Thus; the presence of the Nickel impurities was evidenced by the EDS spectra, depending on the Ni percentage, present in each sample, as it was evidenced by EDS elemental spectra and also by atomic mapping distribution as shown in Figs. 4, 5 and 6.

The AFM topographic images of pure and Ni-doped ZnO thin films are shown in Fig. 7. It has been found that the mean roughness of the Ni doped ZnO thin films found to decrease with the increase in the Ni concentration. For instance, if we compare undoped ZnO with 10% and 12% Ni-doped ZnO, surfaces Root Mean Square (RMS)of 58.1 nm, 28.4 nm, and 25.5 nm are obtained, respectively. As result, 10% and

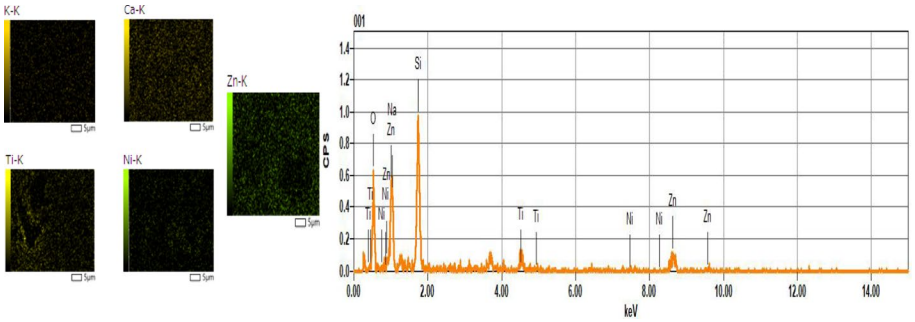

Fig. 5 EDS composition spectra alongside with EDS composition mapping inset, of TiO_2/10%Ni-doped ZnO

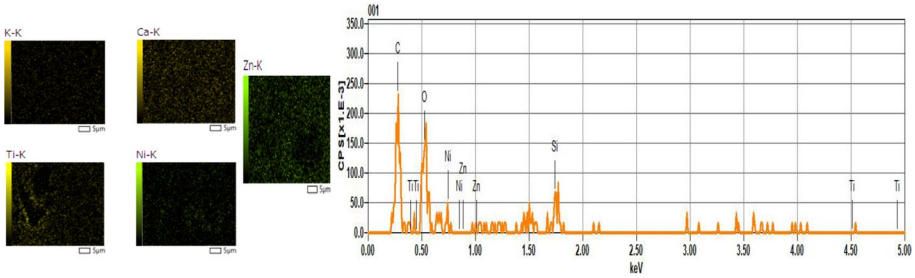

Fig. 6 EDS composition spectra alongside with EDS composition mapping inset, of TiO_2/12%Ni-doped ZnO

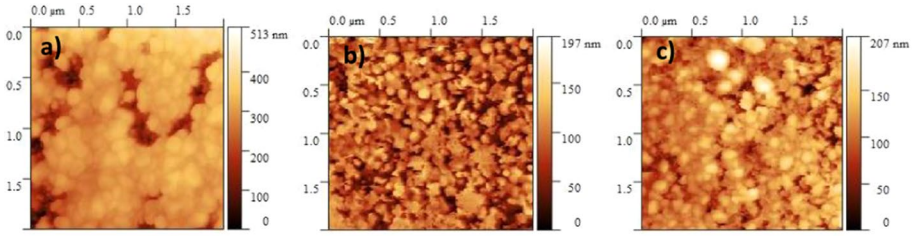

Fig. 7 PeakForce tapping AFM topography for **a** undoped ZnO, **b** 10% Ni-doped ZnO, and **c** 12% Ni-doped ZnO

12% Ni-doped ZnO are demonstrating that the surface layer is more homogeneous than that of ZnO without Ni doping.

The roughness dependencies upon dopants concentration is more likely be due to agglomerations of small crystallites. Note that the roughness is an important parameter that influences on effectiveness and contact resistance, it modifies the performance of optoelectronic device (Ma et al. 2012; Pennec et al. 2012).

4 Optical properties

The absorption of the whole TiO_2/ZnO heterostructure has revealed a decrease in the presence of Ni doping; this decrease in absorbance was observed in ZnO thin films when increasing the Ni doping rate (Owoeye et al. 2019).Additionally, the absorption peaks appear between 250 and 384 nm; illustrating the narrow spikes and demonstrating how Ni doping can significantly reduce absorbance, thereby enhancing transparency and other optical properties; The optical emissions in the subsequent section will then be our primary focus.

The following results show the possibility to fabricate TiO_2 layers on the top of Ni-doped ZnO thin films with the optimal optical qualities required for optoelectronics and LED applications (Rana et al. 2017). Figure 8 shows absorbance spectra of TiO_2/ZnO heterostructure doped from 0 to 12 wt%. The spectra display the same shape for all the films. Moreover, it is observed for the whole studied films, that doping increase leads to absorbance increase from 8 to 12%. This behavior seems to be related to the number of charge carriers increase with higher fillers doping. The system gradually tends towards conductor's behavior. Hence, more states are present for the photon energy to be absorbed thereby increasing the absorption (Markvart and Castañer 2018).The following results demonstrate that it is possible to fabricate TiO_2 layers on top of Ni-doped ZnO thin films with the optimal optical qualities required for applications in optoelectronics and LED (Rana et al. 2017).

The absorbance spectra of a TiO_2/ZnO heterostructure doped from 0 to 12 weight percent are depicted in the figure. For each film, the spectra show the same shape. In addition, it has been observed that an increase in doping results in an increase in absorbance of 8–12%. This behavior seems to be related to the fact that the number of charge carriers grows as the doping increases. The system develops a semiconducting behavior. As a result, the photon energy can be absorbed, resulting in increased absorption (Markvart and Castañer 2018) in more states.

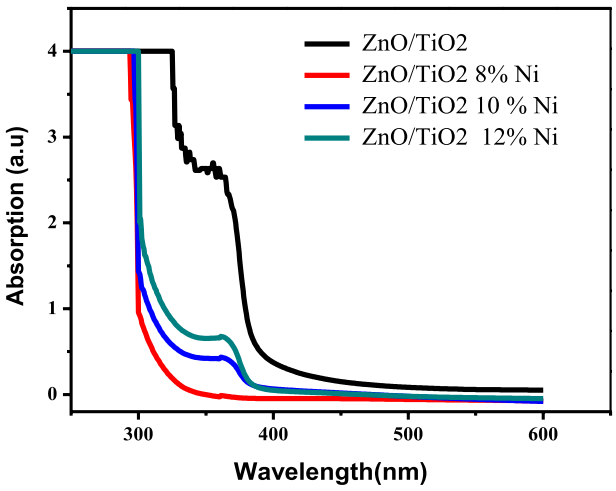

Fig. 8 Absorption spectra in visible range of TiO_2 on Ni(0,8,10,12%)-doped ZnO heterostructures

When a semiconductor is excited above the bandgap energy and as a result of relaxation, luminescence is observed is called photoluminescence, if only photons are emitted, the bandgap will be a "direct" bandgap, If phonons are also emitted with the photons the material will heat up and the band gap is termed as indirect. The phonons emission is due to the defects, impurities, and dopants between CB and VB.Therefore, it is worthy to calculate the band gap energy from photoluminescence emissions data, these calculations will be compared with the band gap value obtained from UV–Visible data.

4.1 Determining the optical band gap from UV–Vis

In semiconductor physics, the bandgap is always one of two types, a direct band gap or an indirect band gap. The minimal-energy state in the conduction band, and the maximal-energy state in the valence band, are all characterized by a certain k-vector in the Brillouin zone. If the k-vectors are the same, it is called a "direct gap". If they are different, it is called an "indirect gap". Direct semiconductors are characterized by having the minimum transition energy to promote an electron from the valence band to the conduction band without a change in the electron momentum (this energy separation is known as the bandgap). However, for indirect semiconductors, excitation at the band gap energy is accompanied by a change in the electron's momentum.

The bandgap energy describes the energy required to excite an electron from the valence band to conduction band. Accurately determine the band Gap energy is important for predicting photonic properties of semiconductors.The absorption coefficient is related to the photon energy and the gap Eg which is determined in the case of a semiconductor by Tauc's relationship (Tauc and Menth 1972)

$$\alpha h\nu = B\left(h\nu - E_g\right)^n \tag{1}$$

where h is Planck's constant, α is the absorption coefficient, ν is the frequency of absorption, B is a constant and sometimes called the band tailing parameter. Eg is the optical energy gap, which is situated between the localized states near the mobility edges according to the density of states model proposed by Mott and Davis (Galperin et al. 1989).The exponent n is a constant, which takes values for direct allowed or indirect allowed transitions as ½ and 2, respectively. Note that, the energy gap or the electron ansition is tightly dependent upon the composition itself, its constituents and its electronic band structure as revealed by Khashan et al. (2014).

From the Tauc plot of Fig. 9, one can clearly see two shoulders, which may be corresponding to different bandgaps related to two oxide systems. ZnO has direct bandgap nature while anatase TiO_2 has indirect nature.

The direct optical energy gap was estimated from the absorption coefficient values using Tauc's procedure. The region showing a steep, linear increase of light absorption with increasing energy is characteristic of semiconductor materials. The x-axis intersection point of the linear fit of the Tauc plot gives an estimate of the band gap energy. The band gap energy is narrowed with the doping process, it was initially 4 eV at 8% Ni and became 3.9 eV at 10% Ni. It was found that the obtained optical gap exhibits a band gap value of 2.91 eV. However, the band gap Eg shifts towards higher values with the rise of metal concentrations, attaining a maximale value of 4 eV for 12% Ni doped ZnO/TiO_2. The obtained results of indirect optical energy gap (Eg) are consistent with those found in some literature works (Morigaki and Ogihara 2017).

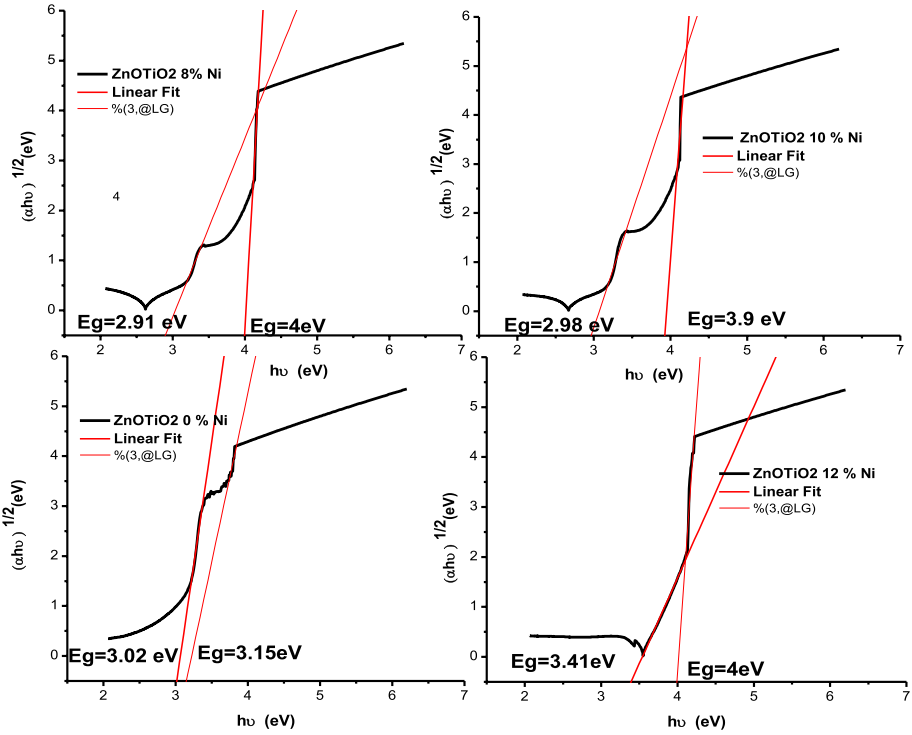

Fig. 9 $(\alpha h\nu)^{1/2}$ versus energy plot for Tauc gap extraction

Thus, in our case this shift is an expected behavior (Hassanien and Akl 2016). The obtained results are in good agreement with other previous works (Tauc 1974; Aly et al. 2012).This seems to have prominent effect on electronic conduction of the studied heterostructure. This direct-to-indirect bandgap crossover, demonstrate a highly tuneable optical properties.

It seems that the effect of growing crystal structure by addition of metallic filler even at ambient temperature, increases lattice quantized vibrations, growing the life and density of the phonons. The phonons are always present in solid at high or low density, depending on its lattice-quantized vibrations. In amorphous solid phonon's effect is vanished by diffusion. However, in the metal particles—periodic structure to a long distance, such the present case, their energy becomes not negligible and they can be absorbed and contribute to the transition. Their exchange with electrons becomes therefore pertinent, allowing indirect interband transitions. Moreover, for such behavior can take place, the electrons must exchange their energy with photons and their momentum with phonons. Note that there is no selection rule for electronic transitions in an indirect gap, unlike the direct gap where the selected rule is the conservation of the momentum. Thus, when the energy of the photon reaches the energy of the direct gap, the absorption will rather be dominated by the direct transitions more than the indirect transitions, since the latter involves a three-particle process: electron, photon and phonon for the conservation of lattice momentum. Therefore, the indirect transitions process can be occurred in two-steps: absorption of energy by the absorption of a photon, followed by the conservation of momentum by emission or

absorption of a phonon. Therefore, it seems that the contribution of phonon is important in the studied thin films with favorited indirect transition of the studied nanofilms.

4.2 Determining the optical band gap from the photoluminescence data

PL spectroscopy depends on the material status, such as defects, impurities, dopants, and the contribution of non-radiative energy transfer to the radiative energy measured by the device. Emission spectra are obtained by exciting the sample at higher energies and observing the resulting emission at lower energies. The exact bandgap is not given for the PL emission, since the emission is not 100% radiative in nature, there is always some non-radiative emission associated with it (Fig. 10).

The bandgap calculated by PL studies is always smaller than the original bandgap. This is because light is absorbed when electrons migrate to the conduction band, leaving holes in the valence band.

Excitons are formed when the Coulomb interaction between electrons and holes is strong, and since they have some associated binding energy, their energy level is slightly lower than that of the conduction band minimum. Therefore, when excitons recombine and emit light, the photon energy measured by PL is slightly smaller than the optical band gap, measured by the absorption of binding energy. Thus, the PL line gives the "band gap minus the exciton binding energy":

$$E_{PL} = E_g - E_{excitons} \tag{2}$$

In fact, this approach is different from the one commonly used. The advantage of this method is that it is not necessary to make an arbitrary choice of low-power excitation to select the PL emission spectrum and its peak energy. This method to accurately determine the Eg band gap has been applied in recently published work (Bleuse 2020).

Several information on material properties such as the gap value can be provided by photoluminescence spectroscopy. In this work, we have used this characterization technique to evaluate the crystal quality of the studied layers and to analyze the effect of dopant and defects on the indirect gap of the titled heterostructure.

The PL spectra of as grown are shown in Fig. 11. They are all taken at the same excitation power and integration time and are hence comparable. The intensities of the spectra are normalized to discuss the difference of the spectral shape, although the total PL intensity increases with an increase in dopant concentration.

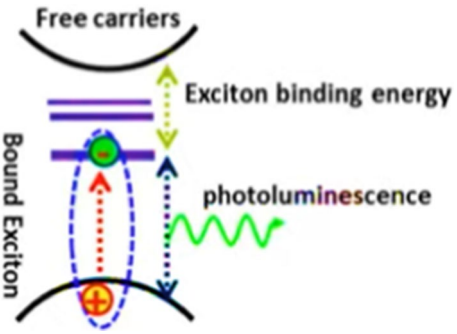

Fig. 10 Radiative vs non-radiative recombination

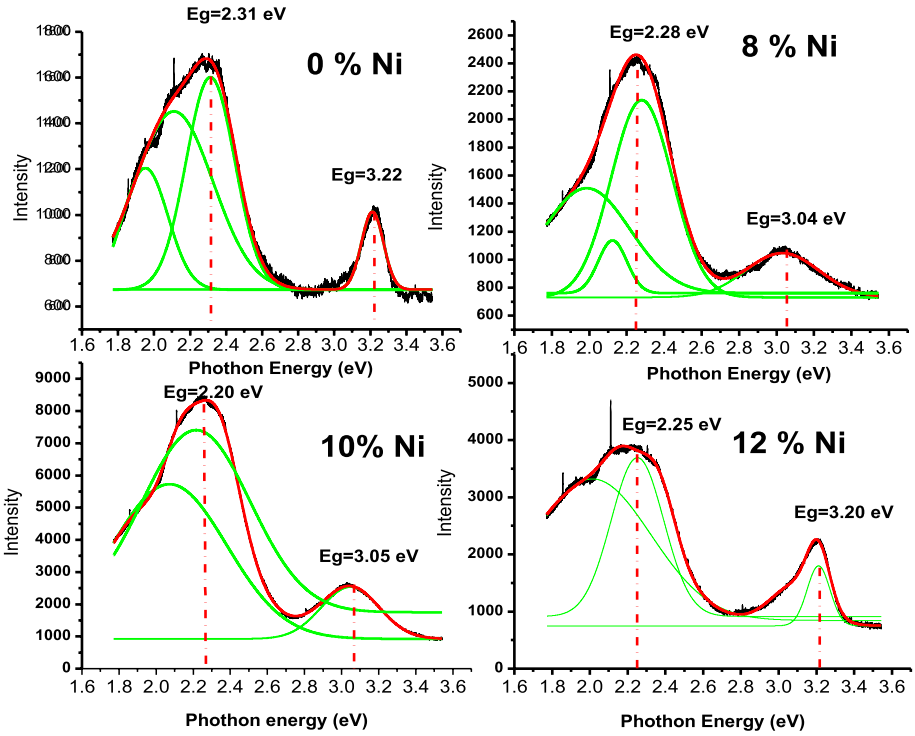

Fig. 11 UV–visible emissions of the Room temperature photoluminescence spectra at room temperature using PL excitation of 3.6 eV, which is bigger than the ZnO and TiO_2, band gaps

It should be noticed that each sample has a broad luminescence band with two Gaussian-type bands with centers at 2.1 and 2.3 eV. The ratio of the band with a center at 2.1 eV decreases as the absorption A increases. It appears that the band with a 2.1 eV center has a close relationship to the oxygen vacancies, this finding has been proven elsewhere (Iijima et al. 2008). Because the spectral structure of the band depends on the doping concentration, another band with a center at 2.3 eV was formed by the recombination of self-trapped excitons (STE) (Sekiya et al. 2000).

Excitons and Ni impurities, are more likely to be responsible for observed changes in peak values at the band edges; this is more likely referred as tuned structures.As our first results, we obtained UV peaks around 3.22 eV from ZnO nanostructures; these peaks are enhanced by increased Ni doping (See Fig. 11). Furthermore, a visible band (405–700 nm) (1.77–3.06 eV) is related to structural defects in ZnO, and an ultraviolet (UV) band (360–375 nm) (3.17–3.3eV) is related to excitons.

To get the value of the wavelength, we extract it from the following relation:

$$E = hv = \frac{h.c}{\lambda} \tag{3}$$

The simplified form of the above equation turns to be written as follows:

$$\lambda = \frac{1240}{E} \tag{4}$$

The obtained deconvoluted spectra clearly confirm that indeed, Anatase TiO_2 has two contributions with two separated spectra namely located at 2.5eV (green emission) and 1.9eV (Red emission); this behavior was observed when TiO_2 films were exposed to O_2 and resulted in a significant reduction of peaks or intensities quenching (Iijima et al. 2008).

The peaks in the range (2.12–2.25 eV) are attributed to TiO_2 Anatase since the ZnO lattice is stacked beneath the TiO_2 thin film. Whereas the Yellow-Green and Violet emissions are caused by oxygen interstitials (2.12–2.25 eV), zinc vacancies (3.03–3.15 eV), zinc interstitials (3.1–3.22 eV), and oxygen vacancy (2.76 -2.95 eV). It is worth noting that the red region in ZnO is commonly associated with oxygen (Alvi et al. 2011). Furthermore, violet emission at 3.10 eV has been observed for Ni 8, 10, and 12% doped ZnO-TiO_2 heterostructures and is attributed to Ni doping due to dislocations and Cottrell atmosphere associated with dislocations (3.15eV). When (0%Ni) and (12%Ni) are compared, the deep-level components are found to be centered in the orange region, while the red components are found to be centered in the red region (See Fig. 12). By facilitating the recombination processes of hole-electrons pairs and more exactly the exchanges between Ni^{2+} cations and O^{2-} anions (Singh et al. 2018), the photoluminescence is enhanced near ultraviolet–visible (UV) region, these results are in agreement with other works (Xie et al. 2015; Xu et al. 2009).

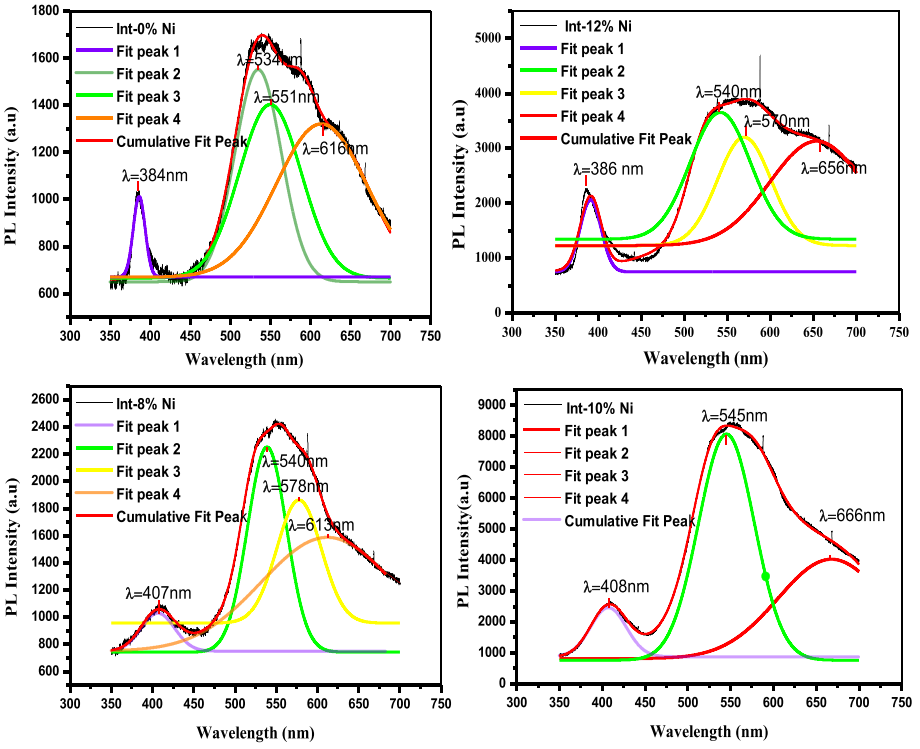

Fig. 12 Deconvolution of photoluminescence PL spectra

5 Conclusion

In summary, we prepared TiO_2/ZnO and TiO_2 on top of Ni(8,10,12%)-doped ZnO heterostructures using two facial deposition methods: dip coating for depositing titanium dioxide thin films on top of as-prepared undoped and Ni(8,10,12%)-doped ZnO, and spray pyrolysis. Furthermore, the microstructural properties of the prepared samples were characterized using Micro Raman spectroscopy, SEM (Scanning electron Microscope), and AFM (Atomic Force Microscopy) at room temperature. Furthermore, the Raman spectra revealed both intensities corresponding to the mean peaks of Wurtzite-ZnO and Anatase-TiO_2. The intensity of the Ni–O bond was also detected and confirmed by the presence of Ni impurities. EDS atomic mapping and elemental spectra specifically indicated the inclusion of Ni as dopants inside the ZnO lattice. In contrast, the AFM in tapping mode verifies the crystalline form of TiO_2 on top of ZnO films, which are all homogenous, smooth, and with minimal roughness. The optical characteristics were measured using two separate techniques. First, the absorbance of the produced heterostructures was evaluated using a spectrophotometer, which indicated that the absorbance decreased as the Ni doping increased. In addition, photoluminescence has shown several emission ranges.

Importantly, we observe the contribution of two oxides, ZnO and TiO_2, and find the role of Ni doping as a key parameter to improve emission over a wide range. Finally, emission tuning is useful for optoelectronic applications such as quantum dot LEDs, multiple quantum wells (MQWs), and electronic light control.

Authors' contribution The authors confirm contribution to the paper as follows: study conception and design: AEH, PFS and EB data collection: HB, analysis and interpretation of results: AEH, MH, AO, AL and MD, draft manuscript preparation: AEH, KN and MH. All authors reviewed the results and approved the final version of the manuscript.

Funding This work has been funded by the Complutense University of Madrid- Banco Santander via project UCM-Santander 2019 (PR87/19-22613) and Complutense University- Comunidad de Madrid via project PR65/19-22464 and the Spanish Ministry of Science, Innovation and Universities via project MINECO/FEDER-MAT2015-65274-R.

Availability of data and materials Data are available from the authors upon reasonable request and with the permission of Springer.

Declarations

Conflict of interest The authors declare that they have no known competing financial interests or personal relationships that could have appeared to influence the work reported in this paper.

Ethical approval Not applicable.

References

Alvi, N.H., ul Hasan, K., Nur, O., Willander, M.: The origin of the red emission in n-zno nanotubes/p-gan white light emitting diodes. Nanoscale Res. Lett. (2011). https://doi.org/10.1186/1556-276X-6-130

Aly, K.A., Abd Elnaeim, A.M., Afify, N., Abousehly, A.M.: Improvement of the electrical properties of Se_3Te_1 thin films by in additions. J. Non-Cryst. Solids **358**(20), 2759–2763 (2012). https://doi.org/10.1016/j.jnoncrysol.2012.06.029

Asib, N.A.M., Afaah, A.N., Aadila, A., Rusop, M., Khusaimi, Z.: Studies of surface morphology and optical properties of ZnO nanostructures grown on different molarities of TiO_2 seed layer. AIP Conf. Proc. (2016). https://doi.org/10.1063/1.4948871

Blanco, E., González-Leal, J., Ramírez-del Solar, M.: Photocatalytic TiO2 sol–gel thin films: optical and morphological characterization. Sol. Energy **122**, 11–23 (2015)

Bleuse, J., Perret, S., Curé, Y., Grenet, L., André, R., et al.: Optical determination of the band gap and band tail of epitaxial $Ag_2ZnSnSe_4$ at low temperature. Phys. Rev. B **102**(19), 195205 (2020)

Chen, P.-Y., Yang, S.-H.: Improved efficiency of perovskite solar cells based on Ni-doped ZnO nanorod arrays and Li salt-doped P3HT layer for charge collection. Opt. Mater. Express **6**(11), 3651 (2016). https://doi.org/10.1364/ome.6.003651

Chen, J., et al.: All solution-processed stable white quantum dot light-emitting diodes with hybrid ZnO@TiO_2 as blue emitters. Sci. Rep. **4**(1), 4085 (2014). https://doi.org/10.1038/srep04085

Cuesta, S., Spies, M., Boureau, V., Donatini, F., Hocevar, M., den Hertog, M.I., Monroy, E.: Effect of bias on the response of GaN axial p-n junction single-nanowire photodetectors. Nano Lett. **19**(8), 5506–5514 (2019). https://doi.org/10.1021/acs.nanolett.9b02040

El Haimeur, A., Makha, M., Bakkali, H., González-Leal, J.M., Blanco, E., Dominguez, M., Voitenko, Z.V.: Enhanced performance of planar perovskite solar cells using dip-coated TiO_2 as electron transporting layer. Sol. Energy (2020). https://doi.org/10.1016/j.solener.2019.11.094

El Haimeur, A., Slassi, A., Pershin, A., Cornil, D., Makha, M., Blanco, E., Dominguez, M., Bakkali, H.: Reducing p-type Schottky contact barrier in metal/ZnO heterostructure through Ni-doping. Appl. Surf. Sci. (2021). https://doi.org/10.1016/j.apsusc.2021.149023

Elilarassi, R., Chandrasekaran, G.: Synthesis and optical properties of Ni-doped zinc oxide nanoparticles for optoelectronic applications. Optoelectron. Lett. **6**(1), 6–10 (2010). https://doi.org/10.1007/s11801-010-9236-y

Frank, O., Zukalova, M., Laskova, B., Kürti, J., Koltai, J., Kavan, L.: Raman spectra of titanium dioxide (anatase, rutile) with identified oxygen isotopes (16, 17, 18). Phys. Chem. Chem. Phys. **14**(42), 14567–14572 (2012). https://doi.org/10.1039/c2cp42763j

Galperin, Y.M., Karpov, V.G., Kozub, V.I.: Localized states in glasses. Adv. Phys. **38**, 669–737 (1989)

Hanada, T.: Basic Properties of ZnO, GaN, and related materials. In: Yao, T., Hong, S.K. (eds.) Oxide and nitride semiconductors. Advances in materials research, vol. 12. Springer, Berlin, Heidelberg (2009). https://doi.org/10.1007/978-3-540-88847-5_1

Harun, K., Hussain, F., Purwanto, A., Sahraoui, B., Zawadzka, A., Mohamad, A.A.: Sol-gel synthesized ZnO for optoelectronics applications: a characterization review. In: Materials research express. Institute of Physics Publishing (2017). https://doi.org/10.1088/2053-1591/aa9e82

Hassanien, A.S., Akl, A.A.: Effect of Se addition on optical and electrical properties of chalcogenide CdSSe thin films. Superlattices Microstruct. **89**, 153–169 (2016). https://doi.org/10.1016/j.spmi.2015.10.044

Hong, S., Han, A., Lee, E.C., Ko, K.-W., Park, J.-H., Song, H.-J., Han, M.-H., Han, C.-H.: A facile and low-cost fabrication of TiO_2 compact layer for efficient perovskite solar cells. Curr. Appl. Phys. **15**(5), 574–579 (2015)

Huang, X., Zhang, L., Wang, S., Chi, D., Chua, S.J.: Solution-grown ZnO films toward transparent and smart dual-color light-emitting diode. ACS Appl. Mater. Interfaces **8**(24), 15482–15488 (2016). https://doi.org/10.1021/acsami.6b03868

Iijima, K., Goto, M., Enomoto, S., Kunugita, H., Ema, K., Tsukamoto, M., Ichikawa, N., Sakama, H.: Influence of oxygen vacancies on optical properties of anatase TiO_2 thin films. J. Lumin. **128**(5–6), 911–913 (2008)

Johansson, W., Peralta, A., Jonson, B., Anand, S., Österlund, L., Karlsson, S.: Transparent TiO_2 and ZnO thin films on glass for UV protection of PV modules. Front. Mater. (2019). https://doi.org/10.3389/fmats.2019.00259

Khashan, K.S., Saimon, J.A., Hassan, A.I.: optical properties of cuo thin films with different concentration by spray pyrolysis method. Eng. Technol. J. **32**(1), 86–93 (2014). https://doi.org/10.30684/etj.32.1B.11

Kityk, I.V., Ebothe, J., Elchichou, A., Addou, M., Bougrine, A., Sahraoui, B.: Linear electro-optics effect in ZnO–F film-glass interface. Phys. Status Solidi **234**(2), 553–562 (2002)

Kulyk, B., Essaidi, Z., Luc, J., Sofiani, Z., Boudebs, G., Sahraoui, B., Kapustianyk, V., Turko, B.: Second and third order nonlinear optical properties of microrod ZnO films deposited on sapphire substrates by thermal oxidation of metallic zinc. J. Appl. Phys. (2007). https://doi.org/10.1063/1.2822461

Look, D.C., Claflin, B.: P-type doping and devices based on ZnO. Physica Status Solidi Basic Res. **241**(3), 624–630 (2004). https://doi.org/10.1002/pssb.200304271

Ma, Z., Tang, Zh., Wang, E., Andersson, M.R., Inganäs, O., Zhang, F.: Influences of surface roughness of ZnO electron transport layer on the photovoltaic performance of organic inverted solar cells. Phys. Chem. C **116**, 24462–24468 (2012)

Manekkathodi, A., Wu, Y.J., Chu, L.W., Gwo, S., Chou, L.J., Chen, L.J.: Integrated optical waveguide and photodetector arrays based on comb-like ZnO structures. Nanoscale **5**(24), 12185–12191 (2013). https://doi.org/10.1039/c3nr03735e

Markvart, T., Castañer, L.: Semiconductor materials and modeling. In: McEvoy's handbook of photovoltaics: fundamentals and applications, pp. 29–57. Elsevier Inc (2018)
Morigaki, K., Ogihara, C.: Amorphous semiconductors: structure, optical, and electrical properties. In: Kasap, S., Capper, P. (eds.) Springer Handbook of electronic and photonic materials. Springer Handbooks, Springer, Cham (2017)
Moyen, E., Kim, J.H., Kim, J., Jang, J.: ZnO nanoparticles for quantum-dot-based light-emitting diodes. ACS Appl. Nano Mater. **3**(6), 5203–5211 (2020). https://doi.org/10.1021/acsanm.0c00639
Nikoobakht, B., Wang, X., Herzing, A., Shi, J.: Scalable synthesis and device integration of self-registered one-dimensional zinc oxide nanostructures and related materials. Chem. Soc. Rev. **42**(1), 342–365 (2013). https://doi.org/10.1039/c2cs35164a
Owoeye, V.A., Ajenifuja, E., Adeoye, E.A., Osinkolu, G.A., Popoola, A.P.: Microstructural and optical properties of Ni-doped ZnO thin films prepared by chemical spray pyrolysis technique. Mater. Res. Express (2019). https://doi.org/10.1088/2053-1591/ab26d9
Pennec, F., Peyrou, D., Leray, D., Pons, P., Plana, R., Courtade, F.: Impact of the surface roughness description on the electrical contactresistance of ohmic switches under low actuation forces. IEEE Trans. Compon. Packag. Manuf. Technol. **2**(1), 85 (2012)
Rahman, F.: Zinc oxide light-emitting diodes: a review. Opt. Eng. **58**(01), 1 (2019). https://doi.org/10.1117/1.oe.58.1.010901
Rajendraprasad Reddy, M., Supriya, V., Sugiyama, M., Reddy, K.T.: Physical investigations on ZnO:Ni layers deposited by spray pyrolysis, In: Conference papers in science 2013. https://doi.org/10.1155/2013/508170.
Rana, A.K., Kumar, Y., Rajput, P., Jha, S.N., Bhattacharyya, D., Shirage, P.M.: Search for origin of room temperature ferromagnetism properties in Ni-doped ZnO nanostructure. ACS Appl. Mater. Interfaces **9**(8), 7691–7700 (2017). https://doi.org/10.1021/acsami.6b12616
Sekiya, T., Ichimura, K., Igarashi, M., Kurita, S.: Absorption spectra of anatase TiO_2 single crystals heat-treated under oxygen atmosphere. J. Phys. Chem. Solids **61**, 1237–1242 (2000)
Singh, H., Kumar, V., Jeon, H.C., et al.: Structural, optical and electrical properties of Ni doped ZnO nanostructures synthesized by solution combustion method. J. Mater. Sci. Mater. Electron. **29**, 1327–1332 (2018). https://doi.org/10.1007/s10854-017-8038-4
Sisman, Z., Bolat, S., Okyay, A.K.: Atomic layer deposition for vertically integrated ZnO thin film transistors: toward 3D high packing density thin film electronics. Physica Status Solidi Curr. Topics Solid State Phys. (2017). https://doi.org/10.1002/pssc.201700128
Son, K.R., Lee, B.R., Kim, T.G.: Chromium/nickel-doped silicon oxide thin-film electrode: mechanism and application to microscale light-emitting diodes. ACS Appl. Mater. Interfaces **10**(48), 40967–40972 (2018). https://doi.org/10.1021/acsami.8b15364
Su, B., He, H., Zhang, H., Pan, X., Ye, Z.: Photoluminescence properties of ZnO/ZnMgO multiple quantum wells under high excitation. Superlattices Microstruct. (2020). https://doi.org/10.1016/j.spmi.2020.106418
Tauc, J.: Amorphous and liquid semiconductors. Plenum, New York (1974)
Tauc, J., Menth, A.: States in the gap. J. Non-Cryst. Solids **10**, 569–585 (1972)
Waszkowska, K., Chtouki, T., Krupka, O., Smokal, V., Figà, V., Sahraoui, B.: Effect of UV-irradiation and ZnO nanoparticles on nonlinear optical response of specific photochromic polymers. Nanomaterials **11**(2), 1–13 (2021). https://doi.org/10.3390/nano11020492
Xie, Q., Zhan, P., Wang, W., Li, Z., Zhang, Z.: Enhanced ultraviolet and visible photoluminescence of ZnO/Zn_2SiO_4/SiO_2/Si multilayer structure. J. Alloys Compd. **642**, 131–135 (2015). https://doi.org/10.1016/j.jallcom.2015.04.032
Xu, L., Shen, H., Li, X., Zhu, R.: Enhanced ultraviolet emission from ZnO thin film covered by TiO_2 nanoparticles. Chin. Opt. Lett. **7**(10), 953 (2009). https://doi.org/10.3788/col20090710.0953
Yin, X., Que, W., Fei, D., Xie, H., He, Z.: Effect of TiO2 shell layer prepared by wet-chemical method on the photovoltaic performance of ZnO nanowires arrays-based quantum dot sensitized solar cells. Electrochim. Acta **99**, 204–210 (2013). https://doi.org/10.1016/j.electacta.2013.03.110
Zawadzka, A., Płóciennik, P., el Kouari, Y., Bougharraf, H., Sahraoui, B.: Linear and nonlinear optical properties of ZnO thin films deposited by pulsed laser deposition. J. Lumin. **169**, 483–491 (2016). https://doi.org/10.1016/j.jlumin.2015.04.020

Authors and Affiliations

Amine El Haimeur[1,3] · Maryama Hammi[2] · Paloma Fernández Sánchez[4] · Hicham Bakkali[1] · Eduardo Ollero Blanco[1] · Abdelmalek Ouannou[5] · Abdellah Laazizi[6] · Manuel Domínguez de la Vega[1] · Khalid Nouneh[3] · Adil Echchelh[7]

✉ Amine El Haimeur
elhaimeur.amine@gmail.com

Maryama Hammi
mar.hammi@yahoo.com

Paloma Fernández Sánchez
arana@fis.ucm.es

Hicham Bakkali
hicham_msn82@hotmail.com

Eduardo Ollero Blanco
eduardo.blanco@gm.uca.es

Abdelmalek Ouannou
a.ouannou@umi.ac.ma

Abdellah Laazizi
abdellah.laazizi@gmail.com

Manuel Domínguez de la Vega
manolo.dominguez@gm.uca.es

Khalid Nouneh
khalid.nouneh@uit.ac.ma

Adil Echchelh
adilechel@gmail.com

[1] Department of Condensed Matter Physics and Institute of Electron Microscopy and Materials, University of Cadiz, Campus Universitario de Puerto Real, Puerto Real, 11510 Cádiz, Spain

[2] Faculty of Sciences, University Mohammed V, BP 1014, Rabat, Morocco

[3] Laboratory of Materials Physics and Subatomic, Faculty of Science, University Ibn Tofail, BP 133-14000, Kenitra, Morocco

[4] Departamento de Física de Materiales, Facultad de Ciencias Físicas, Universidad Complutense de Madrid, Ciudad Universitaria, 28040 Madrid, Spain

[5] Innovation and Technology Transfer Center, Presidency UMI, Meknes, Morocco

[6] Ecole Nationale Superieure d'Arts et Metiers ENSAM., Meknes, Morocco

[7] SITEME Laboratory, Faculty of Sciences, University Ibn Tofail, BP 14000, Kenitra, Morocco